AIAA 2001-2713

Large Injection and Suction Driven Channel Flows with Expanding and Contracting Walls

Chong Zhou and Joseph Majdalani
Marquette University
Milwaukee, WI 53233

31st AIAA Fluid Dynamics Conference
11–14 June 2001
Anaheim, CA

For permission to copy or republish, contact the copyright owner named on the first page. For AIAA-held copyright, write to AIAA, Permissions Department, 1801 Alexander Bell Drive, Suite 500, Reston, VA 20191-4344.

Large Injection and Suction Driven Channel Flows with Expanding and Contracting Walls

C. Zhou* and J. Majdalani†
Marquette University, Milwaukee, WI 53233

In this paper, the incompressible laminar flow is considered inside a porous channel with expanding or contracting walls. While the head-end is closed by a compliant membrane, the downstream end is fully unobstructed. For symmetric injection or suction along the porous and uniformly expanding walls, the Navier-Stokes equations are reduced to a single, nonlinear, ordinary differential equation. The latter is obtained via similarity transformations in both time and space. It is then solved both numerically and asymptotically, using perturbations in the crossflow Reynolds number R. Two separate approaches are presented for each of the injection and suction cases, respectively. For the large injection case, the governing equation is first integrated and the resulting third-order differential equation is solved using the method of variation of parameters. For the large suction case, the governing equation is first simplified near the wall and then solved using successive approximations. Results are then correlated and compared for variations in R and the dimensionless wall expansion rate α. For injection-induced flow, the asymptotic solution becomes more accurate when R/α is increased. Its deviation from the classic sinusoidal profile arising in nonexpanding channels becomes less significant with successive increases in R. Furthermore, expansion of the porous walls is found to promote a more gradual flow turning. Contraction during injection, however, leads to a quicker flow turning accompanied by progressively higher shear stresses and larger axial to normal velocity ratios. For suction-induced flows, faster wall contraction increases the effective Reynolds number $-(\alpha+R)$ and produces more accurate approximations. For the same absolute value of R, the suction-flow approximation tends to be the most accurate of the two and the least sensitive to variations in α. As expected, the suction profile approaches the linear form anticipated in nonexpanding channels. By comparison with the injection-induced flow, suction is characterized by improved accuracy, sharper flow turning, and larger shear.

I. Introduction

STUDIES of porous channel flows have become a recurring topic in fluid mechanics due to the preponderance of related applications. Depending on the application at hand, porous walls have been used in the past to simulate a variety of surface mechanisms. These include natural transpiration, phase sublimation, propellant burning, ablation or sweating, and direct fluid injection or withdrawal. Such mechanisms take place in a number of interesting models of biocirculatory systems, flow filtration, chemical dispensing, rocket propellant combustion, and other membrane separation processes.

Porous channel flow studies appear to have been initiated by Berman[1] in his pioneering work that was concerned with the industrial separation of U_{235} from U_{238} by gas diffusion. In fact, by assuming that the normal velocity component was independent of the streamwise coordinate, Berman was able to reduce the Navier-Stokes equations into a single, nonlinear, fourth-order ODE. His resulting ODE exhibited four boundary conditions and a cross-flow Reynolds number R. The latter was based on the normal injection speed v_w and the channel half-spacing a. For small R, Berman obtained a regularly perturbed expansion. A number of porous channel-flow studies followed thereafter. These were based on either numerical or theoretical approaches. The latter included the methods of integral analysis, averages, curve-fitting, power-series, matched asymptotic expansions, and multiple scales. The reader may in that regard refer to the works of Taylor,[2] Yuan[3]

*Graduate Research Assistant.
†Assistant Professor, Department of Mechanical and Industrial Engineering.
1515 W Wis. Ave, Milwaukee, WI 53233. Phone (414) 288-6877. Fax (414) 288-7082. Email maji@mu.edu.
Copyright © 2001 by C. Zhou and J. Majdalani. Published by the American Institute of Aeronautics and Astronautics, Inc., with permission.

and Terrill[4] (for large injection), Sellars[5] and Terrill[6] (for large suction), Proudman[7] and Shrestha and Terrill[8] (for large R and both equal and dissimilar crossflow velocities), Morduchow[9] and White, Barfield and Goglia[10] (for arbitrary R). Note that Terrill and Shrestha[11] appear to have initiated the study of asymmetric flows caused by different wall permeabilities. Investigations of asymmetric flows and temporal stability issues continue to receive favor in the works of Cox,[12] Zaturska, Drazin and Banks,[13] Taylor, Banks, Zaturska and Drazin[14] and Watson, Banks, Zaturska and Drazin.[15,16]

The spatial stability of steady solutions of the Berman class is another topic that has received much attention in the past. In that regard, one may count Varapaev and Yagodkin,[17] Raithby and Knudsen,[18] Hocking,[19] Sviridenkov and Yagodkin,[20] Brady,[21] and Durlofsky and Brady.[22] In the same vein, the proof of solution multiplicity over different ranges of R has been addressed by Robinson,[23] Skalak and Wang,[24] Shih,[25] Hastings, Lu and MacGillvray,[26] Lu, MacGillvray and Hastings,[27] MacGillvray and Lu,[28] and Lu.[29] Insofar as injection is concerned, only unique and stable symmetrical solutions were shown to exist for the entire range of the injection Reynolds number. This conclusion was first drawn by Skalak and Wang[24] and was later proved rigorously by Shih[25] and Hastings, Lu and MacGillvray.[26] For suction flows with $R < -6.0014$, it was shown that at least one of the symmetric solutions could become unstable to two-dimensional asymmetric disturbances and thus bifurcate into a pair of asymmetric solutions. For a thorough investigation of all possible patterns that could accompany suction flows, the reader is referred to Zaturska, Drazin and Banks.[13] For two-dimensional and three-dimensional considerations, the reader may also find valuable the articles by Cox[12] and Taylor, Banks, Zaturska and Drazin.[14]

In validating the foregoing numerical and theoretical findings, laboratory experiments have also been carried out. Such investigations simulated, in general, steady channel flows through porous sheets. To name a few, one may cite Taylor,[2] Varapaev and Yagodkin,[17] Raithby and Knudsen,[18] and Sviridenkov and Yagodkin.[20] Overall, these studies have indicated that, in the case of wall injection, the asymptotic solutions by Taylor,[2] Yuan[3] or Terrill[4] tended to develop rapidly within the channel. For suction, more than one solution could be observed, with one corresponding to the simple approximation given by Sellars[5] and Terrill.[6]

The purpose of this paper is to extend previous investigations by presenting theoretical solutions for both large injection and suction in a porous channel with expanding or contracting walls. To make headway, we shall limit our scope to symmetric solutions only. In the suction case, the reader is cautioned that our model does not consider asymmetric solutions that may physically exist. To reduce the Navier-Stokes equations, we shall first combine the procedural tools found in Berman,[1] Yuan,[3] Sellars,[5] Terrill,[6] and Goto and Uchida.[30] Using similarity transformations in both space and time we will employ a linearly varying axial velocity and a uniform expansion (or contraction) ratio. This will reduce the Navier-Stokes equations into a single nonlinear equation that can be solved both numerically and asymptotically. Depending on whether injection or suction is present, two separate asymptotic procedures will be implemented to arrive at closed-form approximations. By making the walls motionless, our solutions will be shown to embrace previous formulations as one may restore, from ours, either Yuan's[3] or Sellars'[5] for the large injection and suction cases, respectively. From the asymptotic solutions, closed-form expressions will be obtained for the velocity, pressure and shear stresses that will be collectively used to characterize the flow. Furthermore, comparisons with numerical solutions will demonstrate the accuracy of the asymptotic formulations over a wide range of moderate-to-high Reynolds numbers.

II. Mathematical Model

A porous plenum or chamber can be modeled as a channel of rectangular cross section. In this study, one side of the cross section, representing the distance $2a$ between the porous walls is taken to be smaller than the other two. This enables us to treat the problem as a case of two-dimensional flow. Both sidewalls are assumed to have equal permeability and to expand or contract uniformly at a time-dependent rate $\dot{a}$. Due to the lack of restriction to specify a finite body length L, one may assume a semi-infinite length.[31] In order to accommodate expanding boundaries, the head end is closed by a compliant membrane that is allowed to stretch with channel expansion. At the downstream end, the channel is fully open.

As shown in Fig. 1, a coordinate system may be chosen with the origin at the center of the channel.

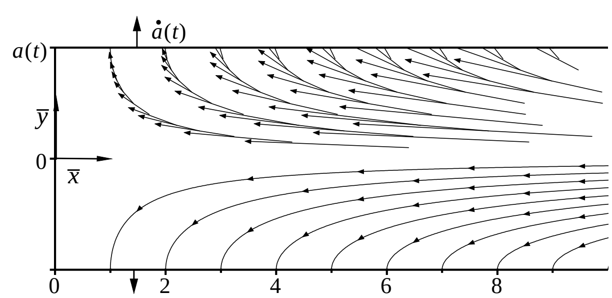

Fig. 1 Two-dimensional channel with expanding (or contracting) porous walls. Vector and streamline plots are depicted in the opposing halves of the solution domain.

Using the over-bar in some cases to denote dimensional variables, we let $\bar{x}$ and $\bar{y}$ be the axial and normal coordinates. The corresponding axial and normal velocity components are defined as $\bar{u}$ and $\bar{v}$. For uniform wall injection and no flow across the midsection plane, symmetry makes it sufficient to limit the investigation over half of the channel, extending from the midplane to the wall ($0 \le \bar{y} \le a$).

For two-dimensional laminar and incompressible flow with no body forces, the differential expressions for mass and momentum conservation can be written as

$$\frac{\partial \bar{u}}{\partial \bar{x}} + \frac{\partial \bar{v}}{\partial \bar{y}} = 0 \tag{1}$$

$$\frac{\partial \bar{u}}{\partial t} + \bar{u}\frac{\partial \bar{u}}{\partial \bar{x}} + \bar{v}\frac{\partial \bar{u}}{\partial \bar{y}} = -\frac{1}{\rho}\frac{\partial \bar{p}}{\partial \bar{x}} + \nu\left(\frac{\partial^2 \bar{u}}{\partial \bar{x}^2} + \frac{\partial^2 \bar{u}}{\partial \bar{y}^2}\right) \tag{2}$$

$$\frac{\partial \bar{v}}{\partial t} + \bar{u}\frac{\partial \bar{v}}{\partial \bar{x}} + \bar{v}\frac{\partial \bar{v}}{\partial \bar{y}} = -\frac{1}{\rho}\frac{\partial \bar{p}}{\partial \bar{y}} + \nu\left(\frac{\partial^2 \bar{v}}{\partial \bar{x}^2} + \frac{\partial^2 \bar{v}}{\partial \bar{y}^2}\right) \tag{3}$$

where ρ, ν, $\bar{p}$, and t are the dimensional density, kinematic viscosity, pressure, and time. The boundary conditions are:

$$\bar{u}(\bar{x},a) = 0 \qquad \bar{v}(a) = -v_{\mathrm{w}} = -A\dot{a} \tag{4}$$

$$\frac{\partial \bar{u}}{\partial \bar{y}}(\bar{x},0) = 0 \qquad \bar{v}(0) = 0 \qquad \bar{u}(0,\bar{y}) = 0\,. \tag{5}$$

At the wall, it is assumed that the fluid inflow velocity v_{w} is independent of position. Additionally, the injection coefficient ($A \equiv v_{\mathrm{w}}/\dot{a}$) that appears in Eq. (4) is a measure of wall permeability.

At this point, the Stokes stream function may be introduced. This is accomplished via

$$\bar{u} = \frac{\partial \bar{\psi}}{\partial \bar{y}}, \qquad \bar{v} = -\frac{\partial \bar{\psi}}{\partial \bar{x}}. \tag{6}$$

Pressure can also be eliminated from the momentum equation by transforming it into the vorticity transport equation. In fact, taking the curl of the momentum equation yields

$$\frac{\partial \bar{\zeta}}{\partial t} + \bar{u}\frac{\partial \bar{\zeta}}{\partial \bar{x}} + \bar{v}\frac{\partial \bar{\zeta}}{\partial \bar{y}} = \nu\left(\frac{\partial^2 \bar{\zeta}}{\partial \bar{x}^2} + \frac{\partial^2 \bar{\zeta}}{\partial \bar{y}^2}\right), \tag{7}$$

where

$$\bar{\zeta} = \frac{\partial \bar{v}}{\partial \bar{x}} - \frac{\partial \bar{u}}{\partial \bar{y}}\,. \tag{8}$$

III. Reduction of the Flow Equations

A. Similar Solution in Space

A similar solution with respect to $\bar{x}$ can be developed from mass conservation. In fact, a simple mass balance suggests that $\bar{v}/\bar{u} = \bar{x}/a$. In view of the boundary conditions given by Eqs. (4) and (5), a similar solution can be developed from the mean-flow stream function. Defining the dimensionless normal coordinate to be $y \equiv \bar{y}/a$, the stream function can be written as

$$\bar{\psi} = \nu h(a)\bar{x}\bar{F}(y,t) \tag{9}$$

where $\bar{F}(y,t)$ is independent of the axial coordinate, and $h(a)$ is some subsidiary function. Inserting Eq. (9) into Eq. (6), the axial and normal velocities can be expressed as

$$\bar{u} = \frac{\nu\bar{x}}{a}h(a)\bar{F}_y\,, \qquad \bar{v} = -\nu h(a)\bar{F}(y,t) \tag{10}$$

where $\bar{F}_y = \partial\bar{F}/\partial y$. Due to the linear spatial dependence, we have $\bar{u}_{\bar{x}\bar{x}} = \bar{v}_{\bar{x}} = 0$. As $\bar{v}$ is independent of $\bar{x}$, the vorticity equation reduces to

$$\bar{\zeta} = -\frac{\partial \bar{u}}{\partial \bar{y}} \tag{11}$$

whereby Eq. (3) collapses into $\bar{p}_{\bar{y}\bar{x}} = 0$. Upon substitution into Eq. (7), one obtains

$$\bar{u}_{\bar{y}t} + \bar{u}\bar{u}_{\bar{y}\bar{x}} + \bar{v}\bar{u}_{\bar{y}\bar{y}} = \nu\bar{u}_{\bar{y}\bar{y}\bar{y}}\,. \tag{12}$$

Inserting Eq. (10) into Eq. (12) gives

$$\left[\frac{\nu\bar{x}}{a^2}h(a)\bar{F}_{\bar{y}\bar{y}}\right]_t + \frac{\nu^2\bar{x}}{a^3}h^2(a)\bar{F}_{\bar{y}}\bar{F}_{\bar{y}\bar{y}} - \frac{\nu^2\bar{x}}{a^3}h^2(a)\bar{F}\bar{F}_{\bar{y}\bar{y}\bar{y}} = \frac{\nu^2\bar{x}}{a^4}h(a)\bar{F}_{\bar{y}\bar{y}\bar{y}\bar{y}}\,. \tag{13}$$

This equation will be dimensionally homogeneous if, and only if

$$\frac{\nu^2\bar{x}}{a^3}h^2(a) \sim \frac{\nu^2\bar{x}}{a^4}h(a) \quad \text{or} \quad h(a) = a^{-1}\,. \tag{14}$$

The axial and normal velocities become

$$\bar{u} = \frac{\nu\bar{x}}{a^2}\bar{F}_y\,, \quad \text{and} \quad \bar{v} = -\frac{\nu}{a}\bar{F}(y,t)\,. \tag{15}$$

B. Governing Equation

In order to solve Eq. (12), one must start by evaluating its partial derivatives. Using $y = \bar{y}/a$ and applying the chain rule to Eq. (15), one obtains

$$\bar{u}_{\bar{y}} = \left(\frac{\nu\bar{x}}{a^2}\bar{F}_y\right)_y \frac{\mathrm{d}y}{\mathrm{d}\bar{y}} = \frac{\nu\bar{x}}{a^3}\bar{F}_{yy} \tag{16}$$

In turn, partial derivatives change into

$$\bar{u}_{\bar{y}\bar{x}} = \frac{\nu}{a^3}\bar{F}_{yy}\,,\ \bar{u}_{\bar{y}\bar{y}} = \frac{\nu\bar{x}}{a^4}\bar{F}_{yyy}\,,\ \bar{u}_{\bar{y}\bar{y}\bar{y}} = \frac{\nu\bar{x}}{a^5}\bar{F}_{yyyy}\,. \tag{17}$$

Recalling that y and a are time-dependent, one may evaluate $\bar{u}_{\bar{y}t}$ as

$$\bar{u}_{\bar{y}t} = \left(\frac{\nu\bar{x}}{a^3}\bar{F}_{yy}\right)_t = \frac{\nu\bar{x}}{a^3}\bar{F}_{yyt} + \frac{\nu\bar{x}}{a^3}\bar{F}_{yyy}\frac{\partial y}{\partial t} - \frac{3\nu\bar{x}\dot{a}}{a^4}\bar{F}_{yy}\,;$$

$$\frac{\partial y}{\partial t} = -\frac{\dot{a}y}{a} \tag{18}$$

By collecting terms, one gets

$$\bar{u}_{\bar{y}t} = \frac{\nu\bar{x}}{a^3}\bar{F}_{yyt} - \frac{\nu\bar{x}\dot{a}}{a^4}y\bar{F}_{yyy} - \frac{3\nu\bar{x}\dot{a}}{a^4}\bar{F}_{yy}\,. \tag{19}$$

By substituting Eq. (17) and Eq. (19) into Eq. (12), a differential equation is developed for $\bar{F}$. This is

$$\bar{F}_{yyyy} + \alpha\left(y\bar{F}_{yyy} + 3\bar{F}_{yy}\right) + \bar{F}\bar{F}_{yyy} - \bar{F}_y\bar{F}_{yy} - a^2\nu^{-1}\bar{F}_{yyt} = 0 \tag{20}$$

where α is the wall expansion ratio defined by

$$\alpha \equiv \frac{\dot{a}a}{\nu}. \qquad (21)$$

Note that the expansion ratio will be positive for expansion and negative for wall contraction. A careful integration of Eq. (20) produces

$$\bar{F}_{yyy} + \alpha\left(y\bar{F}_{yy} + 2\bar{F}_y\right) + \bar{F}\bar{F}_{yy} - \left(\bar{F}_y\right)^2 - a^2\nu^{-1}\bar{F}_{yt} = \lambda\,, \qquad (22)$$

where λ is space-invariant. The boundary conditions given by Eqs. (4)–(5) can be updated into

$$\bar{F}_{yy}(0) = 0 \quad \bar{F}(0) = 0 \quad \bar{F}_y(1) = 0 \quad \bar{F}(1) = R \qquad (23)$$

where R is the crossflow Reynolds number defined by $R \equiv av_{\mathrm{w}}/\nu$. Note that R is positive for injection and negative for suction. Quantities expressed by Eqs. (9), (15), (20) and (23) can be normalized via

$$\psi = \frac{\bar{\psi}}{av_w}\,,\ u = \frac{\bar{u}}{v_w}\,,\ v = \frac{\bar{v}}{v_w}\,,\ x = \frac{\bar{x}}{a}\,,\ F = \frac{\bar{F}}{R} \qquad (24)$$

where F is the characteristic mean-flow function. When this dimensionless set is used, the normalized equations become

$$\psi = xF \qquad (25)$$

$$u = xF_y\,, \qquad v = -F \qquad (26)$$

$$R^{-1}F_{yyy} + \alpha R^{-1}\left(yF_{yy} + 2F_y\right) + FF_{yy} - \left(F_y\right)^2 - \left(a/v_{\mathrm{w}}\right)F_{yt} = \lambda \qquad (27)$$

wherein

$$F_{yy}(0) = 0\,,\ F(0) = 0\,,\ F_y(1) = 0\,,\ F(1) = 1\,. \qquad (28)$$

C. Similar Solution in Space and Time

A similar solution with respect to both space and time can now be developed by precisely following the transformation described by Uchida and Aoki.[31] For constant α and $F = F(y)$, it follows that $F_{yyt} = 0$. To realize this condition, the value of the expansion ratio α must be specified by its initial value

$$\alpha = \frac{\dot{a}a}{\nu} = \frac{\dot{a}_0 a_0}{\nu} = \text{constant}, \qquad (29)$$

where a_0 and $\dot{a}_0$ denote the initial channel height and expansion rate. Forthwith, the temporal similarity transformation can be achieved by integrating Eq. (29) with respect to time. The result is

$$a(t) = a_0\sqrt{1 + 2\nu\alpha t a_0^{-2}}\,. \qquad (30)$$

From Eq. (4), an expression for the injection velocity variation can be determined, provided that the injection coefficient A in Eq. (4) is constant:

$$\frac{\dot{a}(t)}{\dot{a}_0} = \frac{v_{\mathrm{w}}(t)}{v_{\mathrm{w}}(0)} = \left(1 + \frac{2\nu\alpha t}{a_0^2}\right)^{-\frac{1}{2}}. \qquad (31)$$

Under these provisions, Eq. (27) becomes

$$R^{-1}F''' + \alpha R^{-1}\left(yF'' + 2F'\right) + FF'' - \left(F'\right)^2 = \lambda \qquad (32)$$

where a prime denotes differentiation with respect to y. The exact solution becomes contingent upon finding an F that satisfies

$$F''(0) = 0\,,\ F(0) = 0\,,\ F'(1) = 0\,,\ F(1) = 1. \qquad (33)$$

Note that Berman's classic equation[1] is a special case of Eq. (32) that can be obtained by suppressing α.

IV. Solution for the Large Injection Case

For moderate-to-large values of the positive Reynolds number, Eq. (32) can be solved asymptotically. For that purpose, we define $\varepsilon \equiv R^{-1}$ as our perturbation parameter. The problem becomes that of solving

$$\varepsilon F''' + \alpha\varepsilon\left(yF'' + 2F'\right) + FF'' - \left(F'\right)^2 = \lambda \qquad (34)$$

where a small parameter multiplies the highest derivative. Evidently, a regular perturbation expansion of the form $F = F_0 + \varepsilon F_1 + O(\varepsilon^2)$, $\lambda = \lambda_0 + \varepsilon\lambda_1$ can be attempted. In fact, substitution into Eq. (34) gives, at $O(1)$,

$$F_0F_0'' - \left(F_0'\right)^2 = \lambda_0\,, \qquad (35)$$

with $F_0'(1) = 0,\ F_0(1) = 1,\ F_0(0) = 0$. It can be easily verified that the leading-order solution is $F_0 = \sin\theta$, where $\theta = \frac{1}{2}\pi y$ and $\lambda_0 = -\frac{1}{4}\pi^2$.

A. First-order Solution in θ

Terms of $O(\varepsilon)$ can be gathered and separated. The emerging first-order equation is

$$F_0F_1'' - 2F_0'F_{11}' + F_0''F_1 = -F_0''' - 2\alpha F_0' - \alpha y F_0'' + \lambda_1\,. \qquad (36)$$

This needs to be solved while satisfying

$$F_1'(1) = 0,\ F_1(1) = 0,\ F_1(0) = 0\,. \qquad (37)$$

Switching to θ as the independent variable, and using $F_0 = \sin\theta$, Eq. (36) becomes

$$\sin\theta F_1'' - 2\cos\theta F_1' - \sin\theta F_1 = \left(\tfrac{1}{2}\pi - 4\alpha/\pi\right)\cos\theta + (2\alpha/\pi)\theta\sin\theta + \lambda_2\,,$$

$$\lambda_2 = -4\pi^{-2}\lambda_1 \qquad (38)$$

with $$F_1'\left(\tfrac{1}{2}\pi\right) = 0,\ F_1\left(\tfrac{1}{2}\pi\right) = 0,\ F_1(0) = 0\,. \qquad (39)$$

B. Solving by Variation of Parameters

The solution of Eq. (38) must be carefully constructed. First, one can attempt to solve the homogeneous equation,

$$\sin\theta F_1'' - 2\cos\theta F_1' - \sin\theta F_1 = 0\,. \qquad (40)$$

To that end, one independent solution exhibited by Eq. (40) can be guessed to be

$$F_{1H} = \cos\theta\,. \qquad (41)$$

Having determined one independent solution, the method of variation of parameters may be employed. This requires setting

$$F_{1H} = K(\theta)\cos\theta \tag{42}$$

where $K(\theta)$ is unknown. Differentiation gives

$$F_{1H}' = K'\cos\theta - K\sin\theta\,, \tag{43}$$

$$F_{1H}'' = K''\cos\theta - 2K'\sin\theta - K\cos\theta\,. \tag{44}$$

Substitution into Eq. (40) yields

$$K''\sin 2\theta - 4K' = 0\,. \tag{45}$$

Thus K can be determined to be

$$K(\theta) = K_0(\tan\theta - \theta) + K_1\,, \tag{46}$$

where K_0 and K_1 are integration parameters. This completes the expression for the general homogeneous solution

$$F_{1H} = K_0(\sin\theta - \theta\cos\theta) + K_1\cos\theta\,. \tag{47}$$

According to the method of variation of parameters, the two constants K_0 and K_1 must again be allowed to vary with θ. At the outset, Eq. (47) becomes

$$F_1(\theta) = K_0(\theta)(\sin\theta - \theta\cos\theta) + K_1(\theta)\cos\theta\,. \tag{48}$$

The last term needs to be differentiated twice before substitution into Eq. (38). The first differentiation yields

$$F_1' = K_0'(\sin\theta - \theta\cos\theta) + K_0\theta\sin\theta + K_1'\cos\theta - K_1\sin\theta\,. \tag{49}$$

C. Parametric Constraint

At this point, a procedural constraint that binds the derivatives of the variable parameters must be imposed. Our choice is guided by conventional theory that suggests setting

$$K_0'(\sin\theta - \theta\cos\theta) + K_1'\cos\theta = 0\,. \tag{50}$$

Equation (49) becomes

$$F_1' = K_0\theta\sin\theta - K_1\sin\theta\,. \tag{51}$$

Differentiating a second time renders

$$F_1'' = K_0'\theta\sin\theta + K_0(\sin\theta + \theta\cos\theta) - K_1'\sin\theta - K_1\cos\theta\,. \tag{52}$$

We now substitute F_1 and its derivatives, given by Eqs. (48), (51), and (52), back into the complete first-order equation, given by Eq. (38). The result is

$$K_0'\theta\sin^2\theta - K_1'\sin^2\theta = \left(\tfrac{1}{2}\pi - \frac{4\alpha}{\pi}\right)\cos\theta + \frac{2\alpha}{\pi}\theta\sin\theta + \lambda_2\,. \tag{53}$$

Equation (53) contains two unspecified functions, K_0' and K_1'. In order to obtain closure, the constraint introduced in Eq. (50) must be employed alongside Eq. (53). At length, we find that

$$K_0'(\theta) = \left(\tfrac{1}{2}\pi - \frac{4\alpha}{\pi}\right)\frac{\cos^2\theta}{\sin^3\theta} + \frac{2\alpha\theta\cos\theta}{\pi\sin^2\theta} + \frac{\lambda_2\cos\theta}{\sin^3\theta} \tag{54}$$

$$K_1'(\theta) = \frac{2\alpha}{\pi}\left(\frac{\theta^2\cos\theta}{\sin^2\theta} - \frac{\theta}{\sin\theta}\right) + \left(\tfrac{1}{2}\pi - \frac{4\alpha}{\pi}\right)\left(\frac{\theta\cos^2\theta}{\sin^3\theta} - \frac{\cos\theta}{\sin^2\theta}\right) + \lambda_2\left(\frac{\theta\cos\theta}{\sin^3\theta} - \frac{1}{\sin^2\theta}\right) \tag{55}$$

By integrating for the variable parameters, one obtains

$$K_0(\theta) = \left(\frac{2\alpha}{\pi} - \frac{\pi}{4}\right)\frac{\cos\theta}{\sin^2\theta} + \left(\frac{4\alpha}{\pi} - \frac{\pi}{4}\right)\ln\tan\frac{\theta}{2} - \frac{2\alpha\theta}{\pi\sin\theta} - \frac{\lambda_2}{\pi\sin^2\theta} + c_0\,, \tag{56}$$

$$K_1(\theta) = \left(\frac{2\alpha}{\pi} - \frac{\pi}{4}\right)\frac{\theta\cos\theta}{\sin^2\theta} + \left(\frac{\pi}{4} - \frac{2\alpha}{\pi}\right)\frac{1}{\sin\theta} + \left(\frac{4\alpha}{\pi} - \frac{\pi}{4}\right)S(\theta) - \frac{2\alpha\theta^2}{\pi\sin\theta} + \frac{\lambda_2}{2}\left(\frac{\cos\theta}{\sin\theta} - \frac{\theta}{\sin^2\theta}\right) + c_1\,, \tag{57}$$

where c_0 and c_1 are constants and

$$S(\theta) \equiv \int_0^\theta \phi\csc\phi\,\mathrm{d}\phi\,. \tag{58}$$

Inserting Eqs. (56)–(57) into Eq. (48) yields

$$F_1 = -\frac{2\alpha}{\pi}\theta + \left(\frac{4\alpha}{\pi} - \frac{\pi}{4}\right)\left[(\sin\theta - \theta\cos\theta)\ln\tan\tfrac{1}{2}\theta + \cos\theta S(\theta)\right] + \left(c_0 - \tfrac{1}{2}\lambda_2\right)\sin\theta - c_0\theta\cos\theta + c_1\cos\theta\,. \tag{59}$$

Applying the two boundary conditions given by Eq. (39) and making use of $S(0) = 0$, the two constants c_0 and c_1 can be determined. One finds

$$c_0 = \tfrac{1}{2} - 4\alpha\pi^{-2} + \left(8\alpha\pi^{-2} - \tfrac{1}{2}\right)S\left(\tfrac{1}{2}\pi\right),\ c_1 = 0\,,$$
$$\lambda_2 = 2(c_0 + \alpha) = 2\alpha + 1 - 8\alpha\pi^{-2} + \left(16\alpha\pi^{-2} - 1\right)S\left(\tfrac{1}{2}\pi\right). \tag{60}$$

The first-order solution is, therefore,

$$F_1 = -\frac{2\alpha}{\pi}\theta + \left(\frac{\pi}{4} - \frac{4\alpha}{\pi}\right)\left[(\theta\cos\theta - \sin\theta)\ln\tan\tfrac{1}{2}\theta - \cos\theta S(\theta)\right] + \alpha\sin\theta + \left[\left(\tfrac{1}{2} - 8\alpha\pi^{-2}\right)S\left(\tfrac{1}{2}\pi\right) + 4\alpha\pi^{-2} - \tfrac{1}{2}\right]\theta\cos\theta\,. \tag{61}$$

D. Complete Solution

The first-order corrections appearing in Eq. (61) can be combined with the leading-order solution. For added clarity, the resulting function and its derivatives are reproduced below at $O(\varepsilon^2)$:

$$F(\theta) = \sin\theta + \varepsilon\left\{-\frac{2\alpha}{\pi}\theta + \left(\frac{\pi}{4} - \frac{4\alpha}{\pi}\right)\left[(\theta\cos\theta - \sin\theta)\ln\tan\tfrac{1}{2}\theta + \cos\theta S(\theta)\right] + \alpha\sin\theta + \left[\left(\tfrac{1}{2} - 8\alpha\pi^{-2}\right)S\left(\tfrac{1}{2}\pi\right) + 4\alpha\pi^{-2} - \tfrac{1}{2}\right]\theta\cos\theta\right\} \tag{62}$$

$$F'(\theta) = \cos\theta + \varepsilon\left\{\frac{2\alpha}{\pi} - \frac{\pi}{4} + \left(\frac{\pi}{4} - \frac{4\alpha}{\pi}\right)\left[\sin\theta S(\theta) - \theta\sin\theta\ln\tan\tfrac{1}{2}\theta\right] + \alpha\cos\theta + \left[\left(\tfrac{1}{2} - 8\alpha\pi^{-2}\right)S\left(\tfrac{1}{2}\pi\right) + 4\alpha\pi^{-2} - \tfrac{1}{2}\right](\cos\theta - \theta\sin\theta)\right\} \tag{63}$$

$$F''(\theta)=-\sin\theta+\varepsilon\left\{\left(\frac{\pi}{4}-\frac{4\alpha}{\pi}\right)\left[\cos\theta S(\theta)-(\sin\theta\right.\right.$$

$$\left.+\theta\cos\theta)\ln\tan\tfrac{1}{2}\theta\right]-\alpha\sin\theta-\left[\left(\tfrac{1}{2}-8\alpha\pi^{-2}\right)S\left(\tfrac{1}{2}\pi\right)\right.$$

$$\left.\left.+4\alpha\pi^{-2}-\tfrac{1}{2}\right](2\sin\theta+\theta\cos\theta)\right\} \tag{64}$$

$$F'''(\theta)=-\cos\theta+\varepsilon\left\{\left(\frac{\pi}{4}-\frac{4\alpha}{\pi}\right)\left[-\sin\theta S(\theta)-(2\cos\theta\right.\right.$$

$$\left.-\theta\sin\theta)\ln\tan\tfrac{1}{2}\theta-1\right]-\alpha\cos\theta-\left[\left(\tfrac{1}{2}-8\alpha\pi^{-2}\right)S\left(\tfrac{1}{2}\pi\right)\right.$$

$$\left.\left.+4\alpha\pi^{-2}-\tfrac{1}{2}\right](3\cos\theta-\theta\sin\theta)\right\}. \tag{65}$$

Note that, following Eq. (38), primes have been used to denote differentiation with respect to θ. When reverting back to y, one must use $F=F(\frac{1}{2}\pi y)$, $F_y=\frac{1}{2}\pi F'(\theta)$, $F_{yy}=\frac{1}{4}\pi^2F''(\theta)$, $F_{yyy}=\frac{1}{8}\pi^3F'''(\theta)$. At present, it is reassuring to recognize that Eq. (62) reduces to Yuan's formulation[3] by setting $\alpha=0$, and to Taylor's[2] by setting $\varepsilon=0$.

V. Solution for the Large Suction Case

For the large suction case, R is a large negative number and the location of the boundary layer is shifted across the domain. It is therefore necessary to rewrite the governing equation and its boundary conditions. Using primes to denote differentiation with respect to y, one may begin with

$$R^{-1}F'''+\alpha R^{-1}\left(yF''+2F'\right)+FF''-\left(F'\right)^2=\lambda \tag{66}$$

By letting $z=1-y$, Eqs. (66) and (33) can be rewritten as

$$-F'''+\alpha\left(F''-zF''-2F'\right)+R\left[FF''-\left(F'\right)^2\right]=k \tag{67}$$

$$F''(1)=0,\ F(1)=0,\ F'(0)=0,\ F(0)=1, \tag{68}$$

where k is a constant and the prime has been reassigned to z. Since the suction flow is highly dominated by events that take place near the wall, a first approximation to Eq. (67) can be obtained near $z=0$ by utilizing the corresponding boundary conditions in Eq. (68). Thus we find

$$F'''+MF''=-k, \tag{69}$$

where $M\equiv-(\alpha+R)$ is a large positive number. The solution to Eqs. (68)-(69) is

$$F(z)=1+C\left[\frac{M^2z^2}{2}e^{-M}+1-e^{-Mz}-Mz\right], \tag{70}$$

where $$C=\frac{1}{(M-1)+e^{-M}\left[1-\left(M^2/2\right)\right]}. \tag{71}$$

Considering that e^{-M} is close to zero, the form of Eq. (71) suggests a solution of the type

$$F(z)=1+\sum_{j=1}^{\infty}(M-1)^{-j}F_j(z). \tag{72}$$

We find that, by keeping the first three terms, one is able to achieve reasonable accuracy while retaining simplicity of expression. On that account, the regular perturbation expansion becomes

$$F(z)=1+(M-1)^{-1}\left(1-e^{-Mz}-Mz\right)+(M-1)^{-2}F_2(z). \tag{73}$$

where $F_2(z)$ is to be determined. Forthwith, one can insert Eq. (73) into Eq. (67) and collect terms of order $(M-1)^{-2}$. One finds

$$F_2'''+MF_2''=M^3\left(-Mze^{-Mz}-e^{-Mz}\right)+k_2, \tag{74}$$

where k_2 is a constant. At this order, the boundary conditions become

$$F_2''(1)=0,\ F_2(1)=0,\ F_2'(0)=0,\ F_2(0)=0. \tag{75}$$

Direct integration yields

$$F_2=\left(-\frac{M^2z^2}{2}-3Mz\right)e^{-Mz}+\frac{3M}{M-1}\left(1-z-e^{-Mz}\right) \tag{76}$$

wherefrom

$$F(z)=1+(M-1)^{-1}\left(1-e^{-Mz}-Mz\right)-(M-1)^{-2}$$

$$e^{-Mz}\left(\frac{M^2z^2}{2}+3Mz\right)+3(M-1)^{-3}M\left(1-z-e^{-Mz}\right). \tag{77}$$

Principal derivatives are hence

$$F'(z)=M(M-1)^{-1}\left(e^{-Mz}-1\right)+(M-1)^{-2}e^{-Mz}$$

$$\times\left(\frac{M^3z^2}{2}+2M^2z-3M\right)+3M(M-1)^{-3}\left(Me^{-Mz}-1\right) \tag{78}$$

$$F''(z)=-M^2(M-1)^{-1}e^{-Mz}+(M-1)^{-2}e^{-Mz}$$

$$\times\left(3M^3z+2M^2z+5M^2-\frac{M^4z^2}{2}\right)-3M^3(M-1)^{-3}e^{-Mz} \tag{79}$$

$$F'''(z)=M^3(M-1)^{-1}e^{-Mz}+(M-1)^{-2}e^{-Mz}$$

$$\times\left(-2M^3+2M^2-4M^4z+2M^3z-\frac{M^5z^2}{2}\right)$$

$$+3M^4(M-1)^{-3}e^{-Mz}. \tag{80}$$

Recalling that $F'(y)=-F'(z)$, $F''(y)=F''(z)$, and $F'''(y)=-F'''(z)$, the derivatives in terms of y are at hand. It is interesting to note that the solution given originally by Sellars[5] and later improved by Terrill[6] can be reproduced from Eq. (77) by setting $\alpha=0$.

VI. The Velocity Field

A numerical solution for Eqs. (32)-(33) can be readily obtained using a shooting method in conjunction with a seventh-order Runge-Kutta solver. The step size can be chosen to be sufficiently small to produce true values in at least 8 significant digits. With such negligible error, the numerical solution can be used as a benchmark for comparisons with the moderate-to-large suction and injection approximations. This will be performed over a range of crossflow Reynolds numbers and wall expansion rates.

A. Normal Velocity for Constant Expansion and Contraction Rates

Both numeric and asymptotic plots of the normal velocity v (or $-F$) are now shown in Fig. 2 for constant wall expansion ($\alpha = 10$, Fig. 2a) and contraction ($\alpha = -10$, Fig. 2b). In both figures, the solution appears to be sinusoidal for injection and linear for suction. Such behavior is consistent with Yuan's[3] and Sellars'[5] solutions in the absence of wall motion. Wall motion seems to produce a small additional deviation or shifting from the stationary wall solution. While wall expansion appears to increase the effective suction, wall contraction seems to increase the effective injection Reynolds number. This can be illustrated by comparing the suction plots in Figs 2a and 2b. Since $\alpha = 10$ in Fig. 2a, the Reynolds numbers of -50 and -100 lead to effective suction Reynolds numbers (i.e., $M = -(R+\alpha)$ in Eq. (69)) of 40 and 90. In Fig. 2b, the effective Reynolds numbers become 60 and 110. Insofar as the solution sensitivity to α diminishes at higher suction levels, the spacing between suction curves is reduced in Fig. 2b. Overall, wall contraction is found to accelerate asymptotic convergence in the suction case, whereas expansion seems to accelerate convergence in the wall injection formulation. The magnified portions of the graph indicate that asymptotics and numerics coincide for $R \le -50$ and $R \ge 500$. For this reason, theoretical and numerical solutions become indistinguishable outside the range $-50 \le R \le 500$. Since the accuracy associated with the asymptotic expressions improves at higher effective Reynolds numbers, our models may be quite appropriate in the modeling of both hard-blowing and hard-suction surface phenomena.

B. Axial Velocity for Constant Expansion and Contraction Rates

For the same range of R and α, the self-similar axial velocity u/x is now plotted in Fig. 3. By comparison to Fig. 2, similar conclusions can be drawn. For instance, it can be seen that the injection velocity approaches the cosine profile predicted by Yuan[3] while the suction profile becomes progressively flatter as it approaches the plug pattern predicted by Sellars[5] in the absence of wall motion. Here too, the agreement between asymptotics and numerics improves at higher effective Reynolds numbers. In general, this agreement diminishes near the core where a viscous boundary layer involving exponentially small terms is believed to exist (cf. Terrill[32]). While contraction in Fig. 3b aids the overall suction intensity (and therefore convergence), it leads to a more noticeable discrepancy between asymptotics and numerics in the injection case (e.g., $R = 50$). As far as minimizing the asymptotic error is concerned, contraction appears to be favorable

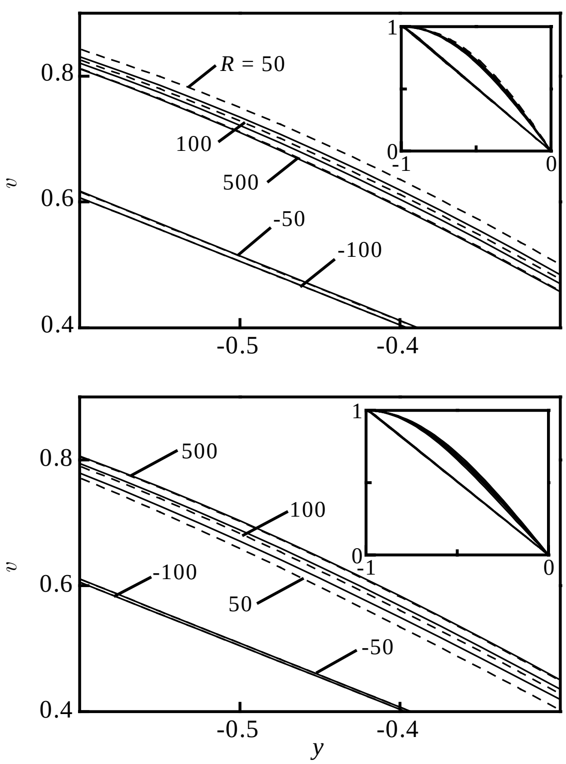

Fig. 2 Comparison between numeric (—) and asymptotic (- - -) solutions for v at a) $\alpha = 10$, and b) $\alpha = -10$; $-100 \le R \le 500$.

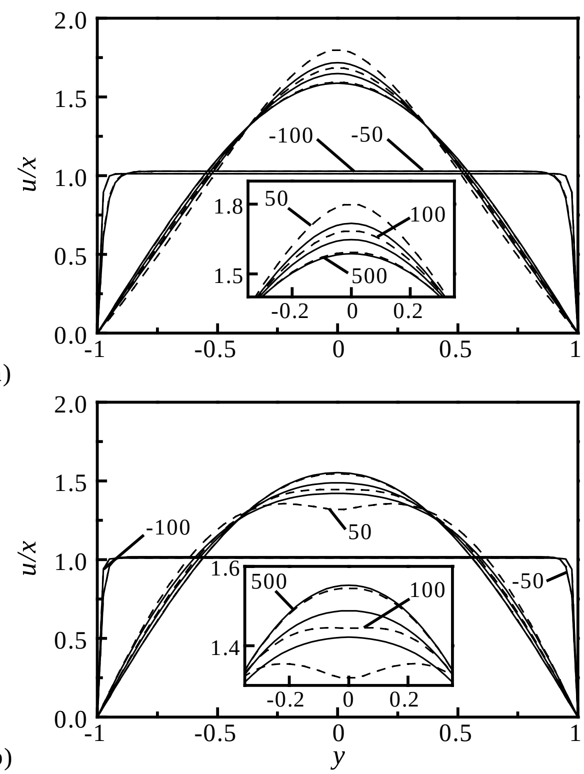

Fig. 3 Comparison between numeric (—) and asymptotic (- - -) solutions for u/x at a) $\alpha = 10$, and b) $\alpha = -10$; $-100 \le R \le 500$.

for suction (since it increases M) and adverse for injection.

C. Axial Velocity for Constant Crossflow Reynolds Numbers

In order to study the field sensitivity to α, the crossflow Reynolds number is now held constant at $R=50$ and $R=-50$ in Figs. 4a and 4b. As α is now varied from -10 to $+10$, both numerical and asymptotic solutions are compared. It thus becomes apparent that, for the same absolute value of the crossflow Reynolds number, the suction-flow approximation is more accurate and less sensitive to variations in α. Even so, the more accurate suction formulation (in Fig. 2b) corresponds to a negative α (i.e., contraction combined with suction). On the other hand, the injection solution becomes less accurate at higher values of α (i.e., as $|\alpha|$ approaches $|R|$). Furthermore, for the same absolute value of α, the injection solution becomes more accurate for positive α (i.e., expansion combined with injection).

D. Improved Convergence in the Suction Flow Approximation

As illustrated in the graphs above, it appears that the suction flow approximation is more accurate than the injection flow solution for the same level of suction or injection. In fact, using the favorable combination of injection $R=100$ and expansion $\alpha=10$, numerics and asymptotics can be compared in Table 1 against the less favorable combination of suction $R=-100$ and $\alpha=10$. Despite the more favorable wall motion in the injection-expansion case, tabulated values indicate that a better agreement can be realized in the suction case. While the precision of the latter extends to 3 significant figures, the injection solution remains limited to 2 digits or less.

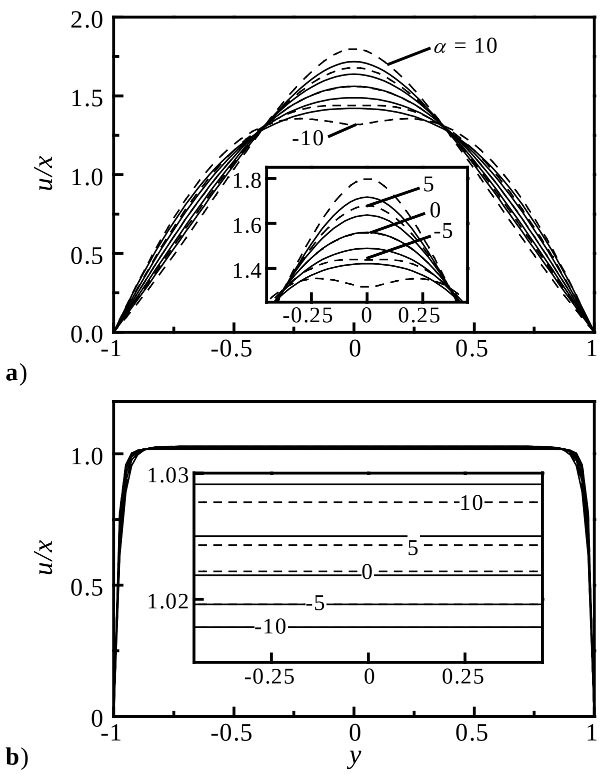

Fig. 4 Comparison between normalized axial velocities obtained from numeric (—) and asymptotic (- - -) solutions over a range of wall regression rates ($-10 \le \alpha \le 10$). The crossflow Reynolds numbers are a) 50 and b) -50.

E. Limitations

Despite the improved accuracy of the suction formulation, it is clear that both asymptotic solutions deteriorate when the expansion or contraction ratios become of the same order as that of the crossflow Reynolds number. The only exception is that of increasing the contraction rate in the suction case. These observations can be explained by first considering the coefficient of the second term in Eq. (34). By recalling that the relevant perturbation solution is based on the condition that $\alpha\varepsilon \ll 1$, it follows that, as α approaches R, the injection formulation becomes less reliable. For suction, on the other hand, since the effective perturbation parameter is based on the reciprocal of M, the expansion can also break down when the sum $\alpha+R$ is no longer large. This will be the case, for instance, when the expansion ratio $\alpha \to -R$ becomes a large positive number. In practice, these limitations are not expected to pose any substantial barriers since $|\alpha|$ seldom exceeds 20.

F. Flow Streamlines

In order to help visualization of the fundamental flow structure, streamlines originating from several discrete locations along the wall are shown in Fig. 5 for several values of R and α. In Fig. 5a, increasing the

F	INJECTION $R=100$		SUCTION $R=-100$	
y	numeric	Eq. (62)	numeric	Eq. (77)
0.0	0.00000	0.00000	0.00000	0.00000
0.1	0.16377	0.16731	0.10117	0.10116
0.2	0.32193	0.32798	0.20234	0.20232
0.3	0.46995	0.47736	0.30351	0.30349
0.4	0.60424	0.61184	0.40468	0.40465
0.5	0.72190	0.72871	0.50585	0.50581
0.6	0.82063	0.82593	0.60702	0.60697
0.7	0.89871	0.90219	0.70819	0.70813
0.8	0.95498	0.95671	0.80937	0.80930
0.9	0.98878	0.98925	0.91053	0.91045
1.0	1.00000	1.00000	1.00000	1.00000

Table 1 Comparison between numeric and asymptotic predictions for F at $\alpha=10$, $R=100$, and $R=-100$.

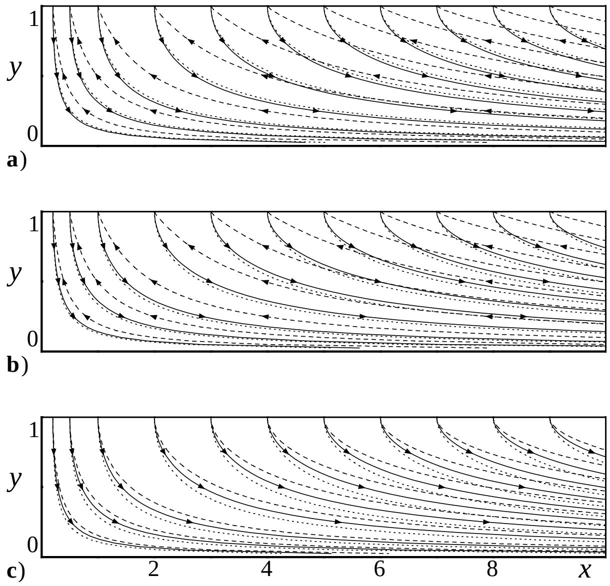

Fig. 5 Mean-flow streamlines for a) $\alpha = 10$ and b) $\alpha = -10$; $R = 50$ (—), -100 (- - -) and 500 ($\cdots$). In c), $R = 50$ and $\alpha = 0$ (—), -20 (- - -), and 20 ($\cdots$).

Reynolds number from 50 to 500 in the presence of wall expansion seems to have a small effect on the flow turning severity. In both cases, the fluid enters the expanding channel almost perpendicularly to the walls. When the flow direction is reversed, a smaller flow suction angle is induced at the wall. By comparison to the gradual turning of the injection-induced flow, the more sudden flow turning associated with the suction case leads to steeper velocity and therefore stress gradients near the wall. When the same comparison is repeated in Fig. 5b with a contraction of $\alpha = -10$, a more severe flow turning pattern is generally observed in both suction and moderate injection cases. The reason is this. As mass is injected more rapidly into the collapsing channel, removal of added mass near the head end requires an increasingly larger axial velocity component. Hence, in order to produce the necessary downstream convection, the relative magnitude of the axial versus normal velocity must increase with faster contraction rates. As explained earlier, for the large injection case (of $R = 500$), the solution becomes much less sensitive to α. On that account, no appreciable flow turning difference can be noted between Fig. 5a and 5b.

The effect of contracting or expanding walls is more clearly isolated in Fig. 5c where α is varied at constant R. By comparison with the $\alpha = 0$ motionless case, a steeper flow turning takes place when the channel walls are in the collapsing mode. This is accompanied by an increase in the relative magnitude of the axial to normal velocity ratio. Conversely, a more gradual flow turning occurs when the walls are in the expansion mode. The consistent reduction in the axial to normal velocity ratio with successive increases in α leads to an interesting hypothetical case. When that ratio reaches zero (for a sufficiently rapid wall regression), the expansion of the walls will exactly negate the effect of flow injection. In that event, the streamlines will remain perpendicular to the wall with a zero axial flow component.

VII. The Stress and Pressure Fields

The constant companions of the velocity field are now considered. These include the shear stress and pressure distributions in both the axial and normal directions.

A. Shear Stress Distribution

To determine the shear stress, one may begin by considering Newton's law for viscosity, vi.

$$\bar{\tau} = \mu\left(\frac{\partial \bar{v}}{\partial \bar{x}} + \frac{\partial \bar{u}}{\partial \bar{y}}\right). \tag{81}$$

Inserting the velocity into Eq. (81) renders

$$\bar{\tau} = \frac{\rho \nu^2 \bar{x}}{a^3} \bar{F}_{yy}. \tag{82}$$

The shear stress may be made dimensionless by using the dynamic pressure as a reference. At the outset,

$$\tau = \frac{\bar{\tau}}{\rho v_{\mathrm{w}}^2} = \varepsilon x F_{yy}. \tag{83}$$

This simple formulation leads to a useful expression for the stress at the wall, namely, to $\tau_{\mathrm{w}} = \varepsilon x F_{yy}(1)$.

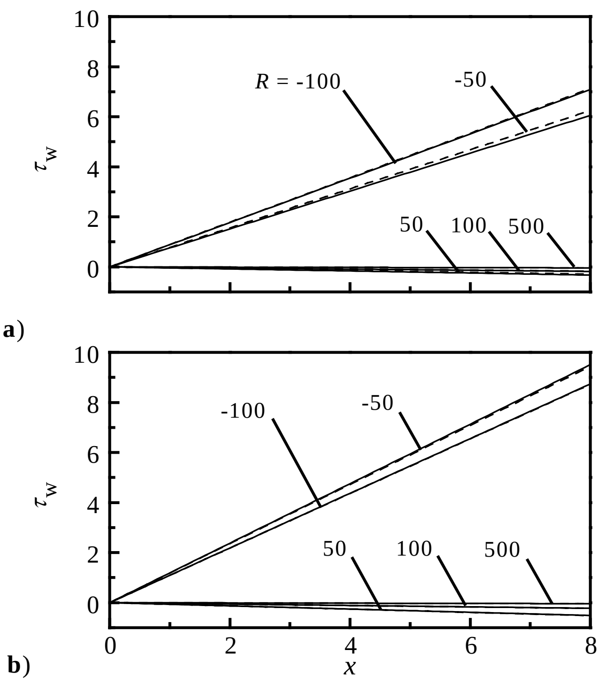

Fig. 6 Comparison between numeric (—) and asymptotic (- - -) wall shear stresses for a) $\alpha = 10$ and b) $\alpha = -10$; $-100 \le R \le 500$.

Forthwith, asymptotic and numerical predictions stemming therefrom can be compared in Fig. 6. In addition to the fair agreement between numerics and asymptotics, one may note a significant shear stress increase in the wall suction case. This increase becomes even more pronounced in Fig. 6b when the walls are in contraction. The increased τ_w for suction flows is consistent with the velocity field description and may be attributed to the increased flow turning severity and steeper velocity gradients near the wall. For injection, the shear stress is negative due to the reversal in axial flow direction. It also decreases at higher Reynolds numbers since, as R becomes larger, the role of viscosity diminishes, the viscous layer becomes thinner and further distanced from the wall (cf. Proudman[7]), and the shear at the wall becomes less appreciable. Here too, the agreement between asymptotics and numerics improves at large R.

B. Normal Pressure Drop

In order to determine the normal pressure drop, one can begin by substituting Eq. (15) into Eq. (3). Since $y = y(t)$, derivatives must be carefully manipulated. To proceed, one first evaluates

$$\frac{\partial \bar{v}}{\partial t} = \frac{\nu^2\alpha}{a^3}\left(\bar{F} + y\bar{F}_y\right),\ \frac{\partial \bar{v}}{\partial \bar{x}} = 0,\ \frac{\partial^2 \bar{v}}{\partial \bar{x}^2} = 0,$$

$$\bar{v}\frac{\partial \bar{v}}{\partial \bar{y}} = \frac{\nu^2}{a^3}\bar{F}\bar{F}_y,\ \frac{\partial^2 \bar{v}}{\partial \bar{y}^2} = -\frac{\nu}{a^3}\bar{F}_{yy}. \qquad (84)$$

Following substitution into Eq. (3), a simple rearrangement yields

$$p_y = -\left[\varepsilon F_{yy} + FF_y + \alpha\varepsilon\left(F + yF_y\right)\right]; \qquad p \equiv \frac{\bar{p}}{\rho v_w^2} \quad (85)$$

The normal pressure distribution can now be determined by integrating Eq. (85) with the boundary conditions given by Eq. (33). Letting p_c be the centerline pressure, one may start with

$$\int_{p_c}^{p(y)} \mathrm{d}p = \int_0^y -\left[\varepsilon F_{yy} + FF_y + \alpha\varepsilon\left(F + yF_y\right)\right]\mathrm{d}y. \quad (86)$$

Recognizing that $FF_y = \frac{1}{2}(F^2)_y$, and $(F + yF_y) = (yF)_y$, one may substitute these relationships into Eq. (86). Subsequent integration yields

$$\Delta p_n \equiv p(y) - p_c = \varepsilon F_y(0) - \left(\varepsilon F_y + \tfrac{1}{2}F^2 + \alpha\varepsilon yF\right). \quad (87)$$

Figures 7a and 7b illustrate the pressure drop for $R = 50$ and $R = -50$. As α is varied from -20 to $+20$, we note that the pressure drop increases with α for injection (Fig. 7a), but decreases for suction (Fig. 7b). We also note that, except for injection combined with wall contraction, the absolute pressure drop is largest near the walls. For $R = 50$ and negative α, the maximum (absolute) pressure drop occurs somewhere between the midsection plane and the wall. Overall, the asymptotic approximation appears to hold quite well up to $|\alpha| = 20$ which is of the same order as R. We also

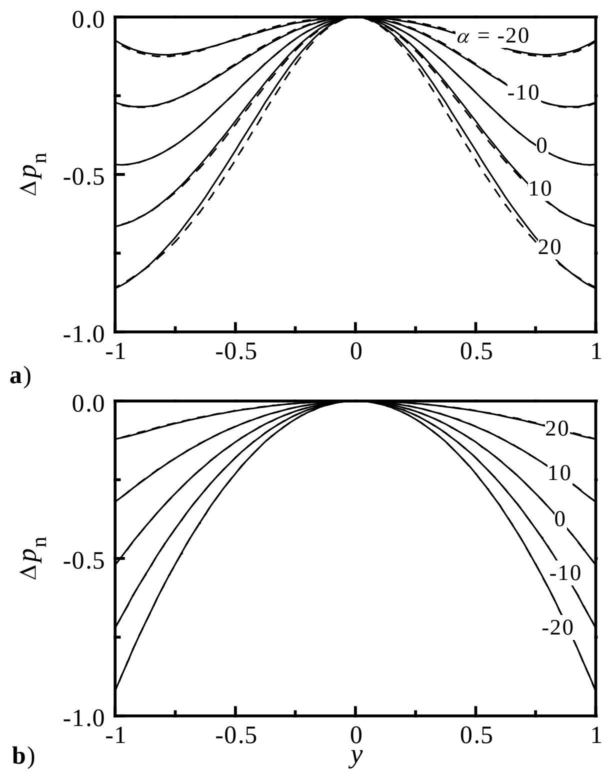

Fig. 7 Comparison between numeric (—) and asymptotic (- - -) pressure drops in the normal direction for a) $R = 50$, and b) $R = -50$; $-20 \le \alpha \le 20$.

note that, for injection and small $\varepsilon\alpha$ in Fig. 7a, the pressure gradient p_y is near zero at the wall. This is consistent with the behavior of Taylor's ideal profile.[2]

C. Axial Pressure Drop

Using

$$\bar{u}_t = \frac{\nu\bar{x}}{a^2}\bar{F}_{yy}\frac{\partial y}{\partial t} - \frac{2\nu\bar{x}\dot{a}}{a^3}\bar{F}_y, \qquad (88)$$

substitution into Eq. (2) leads to the axial pressure gradient. We thus find

$$p_x = x\left[\varepsilon F_{yyy} + FF_{yy} + \left(F_y\right)^2 + \alpha\varepsilon\left(2F_y + yF_{yy}\right)\right]. \quad (89)$$

Subsequent integration gives the axial pressure distribution at any streamwise location,

$$\Delta p_a = \tfrac{1}{2}x^2\left[\varepsilon F_{yyy} + FF_{yy} + \left(F_y\right)^2 + \alpha\varepsilon\left(2F_y + yF_{yy}\right)\right]. \quad (90)$$

We find Δp_a to vary slowly in the axial direction. The agreement between asymptotics and numerics is also improved with $|R|$.

VIII. Conclusions

In this article, an exact similarity solution to the Navier-Stokes equations is presented. The problem arises in the context of a fluid entering a porous channel with moving walls. The similarity transformations in space and time convert the momentum equation into a single, nonlinear, differential equation. It can be easily verified that the resulting equation reduces to the classic Berman equation for a channel with stationary walls. Closed-form solutions obtained using regular perturbations and the method of variation of parameters are shown to coincide with the numerical solution over a useful range of parameters. Due to their adequate accuracy, the explicit formulations presented here are practically equivalent to the exact solution over a range of moderate-to-high Reynolds numbers. When injection is increased, the effect of varying the expansion rate becomes less pronounced. Larger values of R/α and $(R+\alpha)$ improve the accuracy of the asymptotic approximations in injection and suction-induced flows, respectively. Their improved accuracy makes them suitable for modeling the hard-blowing or hard-suction phenomena.

For injection-induced flows, increasing the Reynolds number is also found to accelerate flow turning and to increase the ratio of axial to normal velocities. Conversely, increasing wall expansion seems to inhibit flow turning and decrease the shear stress at the wall. For injection Reynolds numbers in excess of 500, our viscous solution approaches Taylor's inviscid sinusoidal profile provided that the expansion rate remains reasonably small. Similarly, for suction Reynolds numbers below -50, our asymptotic approximation approaches Sellars' linear profile. As such, our current formulations embrace former solutions presented by Taylor,[2] Yuan,[2] and Terrill[4] for injection, and by Sellars[5] and Terrill[6] for suction in nonexpanding channels.

References

[1]Berman, A. S., "Laminar Flow in Channels with Porous Walls," *Journal of Applied Physics,* Vol. 24, No. 9, 1953, pp. 1232-1235.

[2]Taylor, G. I., "Fluid Flow in Regions Bounded by Porous Surfaces," *Proceedings of the Royal Society, London, Series A,* Vol. 234, No. 1199, 1956, pp. 456-475.

[3]Yuan, S. W., "Further Investigation of Laminar Flow in Channels with Porous Walls," *Journal of Applied Physics,* Vol. 27, No. 3, 1956, pp. 267-269.

[4]Terrill, R. M., "Laminar Flow in a Uniformly Porous Channel with Large Injection," *The Aeronautical Quarterly,* Vol. 16, 1965, pp. 323-332.

[5]Sellars, J. R., "Laminar Flow in Channels with Porous Walls at High Suction Reynolds Numbers," *Journal of Applied Physics,* Vol. 26, No. 4, 1955, pp. 489-490.

[6]Terrill, R. M., "Laminar Flow in a Uniformly Porous Channel," *The Aeronautical Quarterly*, Vol. 15, 1964, pp. 299-310.

[7]Proudman, I., "An Example of Steady Laminar Flow at Large Reynolds Number," *Journal of Fluid Mechanics,* Vol. 9, No. 4, 1960, pp. 593-612.

[8]Shrestha, G. M., and Terrill, R. M., "Laminar Flow with Large Injection through Parallel and Uniformly Porous Walls of Different Permeability," *Quarterly Journal of Mechanics and Applied Mathematics,* Vol. 21, No. 4, 1968, pp. 413-432.

[9]Morduchow, M., "On Laminar Flow through a Channel or Tube with Injection: Application of Method of Averages," *Quarterly Journal of Applied Mathematics,* Vol. 14, No. 4, 1957, pp. 361-368.

[10]White, F. M., Jr., Barfield, B. F., and Goglia, M. J., "Laminar Flow in a Uniformly Porous Channel," *Transactions of the American Society of Mechanical Engineers: Journal of Applied Mechanics, Series E,* Vol. 25, 1958, pp. 613-617.

[11]Terrill, R. M., and Shrestha, G. M., "Laminar Flow through Parallel and Uniformly Porous Walls of Different Permeability," *Journal of Applied Mathematics and Physics (ZAMP),* Vol. 16, 1965, pp. 470-482.

[12]Cox, S. M., "Two-Dimensional Flow of a Viscous Fluid in a Channel with Porous Walls," *Journal of Fluid Mechanics,* Vol. 227, 1991, pp. 1-33.

[13]Zaturska, M. B., Drazin, P. G., and Banks, W. H. H., "On the Flow of a Viscous Fluid Driven Along a Channel by Suction at Porous Walls," *Fluid Dynamics Research,* Vol. 4, No. 3, 1988, pp. 151-178.

[14]Taylor, C. L., Banks, W. H. H., Zaturska, M. B., and Drazin, P. G., "Three-Dimensional Flow in a Porous Channel," *Quarterly Journal of Mechanics and Applied Mathematics*, Vol. 44, No. 1, 1991, pp. 105-133.

[15]Watson, E. B. B., Banks, W. H. H., Zaturska, M. B., and Drazin, P. G., "On Transition to Chaos in Two-Dimensional Channel Flow Symmetrically Driven by Accelerating Walls," *Journal of Fluid Mechanics,* Vol. 212, 1990, pp. 451-485.

[16]Watson, P., Banks, W. H. H., Zaturska, M. B., and Drazin, P. G., "Laminar Channel Flow Driven by Accelerating Walls," *European Journal of Applied Mathematics,* Vol. 2, 1991, pp. 359-385.

[17]Varapaev, V. N., and Yagodkin, V. I., "Flow Stability in a Channel with Porous Walls," *Fluid Dynamics,* Vol. 4, No. 5, 1969, pp. 91-95.

[18]Raithby, G. D., and Knudsen, D. C., "Hydrodynamic Development in a Duct with Suction and Blowing," *Transactions of the American Society of Mechanical Engineers: Journal of Applied Mechanics, Series E,* Vol. 41, 1974, pp. 896-902.

[19]Hocking, L. M., "Non-Linear Instability of the Asymptotic Suction Velocity Profile," *Quarterly Journal of Mechanics and Applied Mathematics,* Vol. 28, No. 3, 1975, pp. 341-353.

[20]Sviridenkov, A. A., and Yagodkin, V. I., "Flow in the Initial Sections of Channels with Permeable Walls," *Fluid Dynamics,* Vol. 11, No. 5, 1976, pp. 689-693.

[21]Brady, J. F., "Flow Development in a Porous Channel or Tube," *The Physics of Fluids,* Vol. 27, No. 5, 1984, pp. 1061-1067.

[22]Durlofsky, L., and Brady, J. F., "The Spatial Stability of a Class of Similarity Solutions," *The Physics of Fluids,* Vol. 27, No. 5, 1984, pp. 1068-1076.

[23]Robinson, W. A., "The Existence of Multiple Solutions for the Laminar Flow in a Uniformly Porous Channel with Suction at Both Walls," *Journal of Engineering Mathematics,* Vol. 10, No. 1, 1976, pp. 23-40.

[24]Skalak, F. M., and Wang, C.-Y., "On the Nonunique Solutions of Laminar Flow through a Porous Tube or Channel," *SIAM Journal on Applied Mathematics,* Vol. 34, No. 3, 1978, pp. 535-544.

[25]Shih, K.-G., "On the Existence of Solutions of an Equation Arising in the Theory of Laminar Flow in a Uniformly Porous Channel with Injection," *SIAM Journal on Applied Mathematics,* Vol. 47, No. 3, 1987, pp. 526-533.

[26]Hastings, S. P., Lu, C., and MacGillivray, A. D., "A Boundary Value Problem with Multiple Solutions from the Theory of Laminar Flow," *SIAM Journal on Mathematical Analysis,* Vol. 23, No. 1, 1992, pp. 201-208.

[27]Lu, C., MacGillivray, A. D., and Hastings, S. P., "Asymptotic Behaviour of Solutions of a Similarity Equation for Laminar Flows in Channels with Porous Walls," *IMA Journal of Applied Mathematics,* Vol. 49, 1992, pp. 139-162.

[28]MacGillivray, A. D., and Lu, C., "Asymptotic Solution of a Laminar Flow in a Porous Channel with Large Suction: A Nonlinear Turning Point Problem," *Methods and Applications of Analysis,* Vol. 1, No. 2, 1994, pp. 229-248.

[29]Lu, C., "On the Asymptotic Solution of Laminar Channel Flow with Large Suction," *SIAM Journal on Mathematical Analysis,* Vol. 28, No. 5, 1997, pp. 1113-1134.

[30]Goto, M., and Uchida, S., "Unsteady Flows in a Semi-Infinite Expanding Pipe with Injection through Wall," *Transactions of the Japan Society for Aeronautical and Space Sciences,* Vol. 33, No. 9, 1990, pp. 14-27.

[31]Uchida, S., and Aoki, H., "Unsteady Flows in a Semi-Infinite Contracting or Expanding Pipe," *Journal of Fluid Mechanics,* Vol. 82, No. 2, 1977, pp. 371-387.

[32]Terrill, R. M., "On Some Exponentially Small Terms Arising in Flow through a Porous Pipe," *Quarterly Journal of Mechanics and Applied Mathematics,* Vol. 26, No. 3, 1973, pp. 347-354.